Electrocatalysis

International Edition: DOI: 10.1002/anie.201506727
German Edition: DOI: 10.1002/ange.201506727

Ultrafine Molybdenum Carbide Nanoparticles Composited with Carbon as a Highly Active Hydrogen-Evolution Electrocatalyst

*Ruguang Ma, Yao Zhou, Yongfang Chen, Pengxi Li, Qian Liu, and Jiacheng Wang**

Abstract: *The replacement of platinum with non-precious-metal electrocatalysts with high efficiency and superior stability for the hydrogen-evolution reaction (HER) remains a great challenge. Herein, we report the one-step synthesis of uniform, ultrafine molybdenum carbide (Mo_2C) nanoparticles (NPs) within a carbon matrix from inexpensive starting materials (dicyanamide and ammonium molybdate). The optimized catalyst consisting of Mo_2C NPs with sizes lower than 3 nm encapsulated by ultrathin graphene shells (ca. 1–3 layers) showed superior HER activity in acidic media, with a very low onset potential of −6 mV, a small Tafel slope of 41 mV dec^{-1}, and a large exchange current density of 0.179 mA cm^{-2}, as well as good stability during operation for 12 h. These excellent properties are similar to those of state-of-the-art 20 % Pt/C and make the catalyst one of the most active acid-stable electrocatalysts ever reported for HER.*

Water splitting by electrolysis to produce hydrogen has attracted much attention, because hydrogen, as a clean, sustainable energy source, is one of the most promising alternatives to fossil fuels.[1] Platinum is the most active and catalytically stable catalyst for the hydrogen-evolution reaction (HER, $2H^+ + 2e^- \rightarrow H_2$),[2] but its scarcity and high cost make it impractical for global-scale applications. Much effort has been made to develop cost-effective, transition-metal-based, non-platinum electrocatalysts,[3] such as tungsten-,[4] molybdenum-,[5] cobalt-,[6] iron-,[7] and nickel-based materials;[8] however, most of these materials have had a large overpotential (η) of 100–200 mV.

Molybdenum carbide (Mo_2C) materials are considered to be promising HER electrocatalysts owing to their low cost, high chemical stability, and high similarity to platinum-based catalysts.[3b,5d,9] The activity of Mo_2C can be improved by introducing other elements, such as nitrogen, which may tune the electronic state of Mo active sites in a desirable way.[10] The construction of various nanostructures (e.g. nanooctahedrons, nanowires (NWs), nanoparticles (NPs)) also can improve the HER activity of MoC_2 owing to the enhanced exposure of surface active sites.[5d,6c,9b,c,10] However, it is still a large challenge to controllably synthesize Mo_2C NPs with ultrasmall sizes because of the inevitable aggregation and/or excessive growth of Mo_2C NPs at high reaction temperatures, and the ready oxidation of the surface of Mo_2C NPs to MoO_x species when exposed to air. The former effect leads to a low density of active sites, whereas the latter results in poor electrical transport, both of which can limit the HER performance of Mo_2C NPs.[9a,10]

Herein, we describe a one-step protocol for the synthesis of ultrafine Mo_2C NPs uniformly embedded within a carbon matrix (MCNs@carbon). The resulting material acted as a highly active and stable non-platinum HER electrocatalyst with an extremely low onset potential (U_{onset}) of −6 mV, a small overpotential of 78 mV to reach 10 mA cm^{-2} (η_{10}), a small Tafel slope of 41 mV dec^{-1}, and a large exchange current density (j_0) of 0.179 mA cm^{-2}, as well as good stability over 12 h during operation in 0.5 M H_2SO_4. To the best of our knowledge, the present material MCNs@carbon is one of most active transition-metal-based electrocatalysts for HER.[3a,11]

To synthesize MCNs@carbon, we simply heated a mixture of dicyanamide (DCA) and ammonium molybdate at 400 °C to give graphitic carbon nitride (g-C_3N_4) containing MoO_x species (MoO_x@g-C_3N_4), and annealed the resulting material at 800 °C (Figure 1 a; see the Supporting Information for details). The evolution of the color of the sample from white to black indicated the formation of carbon and/or Mo_2C at 800 °C (Figure 1 b–d), as further confirmed by XRD patterns (see Figure S1 in the Supporting Information). The very broad peaks indicate that the Mo_2C nanoparticles have

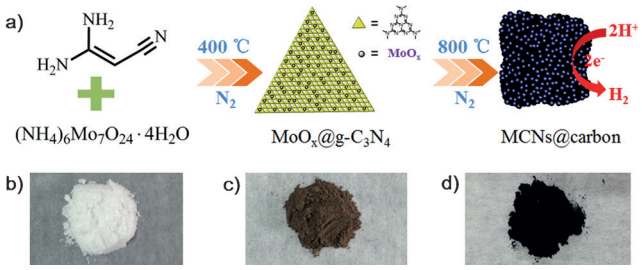

Figure 1. a) Procedure for the synthesis of MCNs@carbon as a non-platinum HER electrocatalyst. b–d) Digital photographs of a mixture of DCA and ammonium molybdate (b), MoO_x@g-C_3N_4 (c), and MCNs@carbon (d).

[*] R. Ma, Y. Zhou, Y. Chen, P. Li, Prof. Q. Liu, Prof. J. Wang
State Key Laboratory of High Performance Ceramics and Superfine Microstructure, Shanghai Institute of Ceramics
Chinese Academy of Sciences
1295 Dingxi Road, Shanghai 200050 (P. R. China)
E-mail: jiacheng.wang@mail.sic.ac.cn
R. Ma, Y. Zhou, Prof. Q. Liu, Prof. J. Wang
Innovation Center for Inorganic Materials Genomic Science
Shanghai Institute of Ceramics, Shanghai 200050 (P. R. China)
and
Shanghai Materials Genome Institute, Shanghai 200444 (P. R. China)
Y. Chen
University of the Chinese Academy of Sciences
Beijing 100049 (P. R. China)

Supporting information for this article is available on the WWW under http://dx.doi.org/10.1002/anie.201506727.

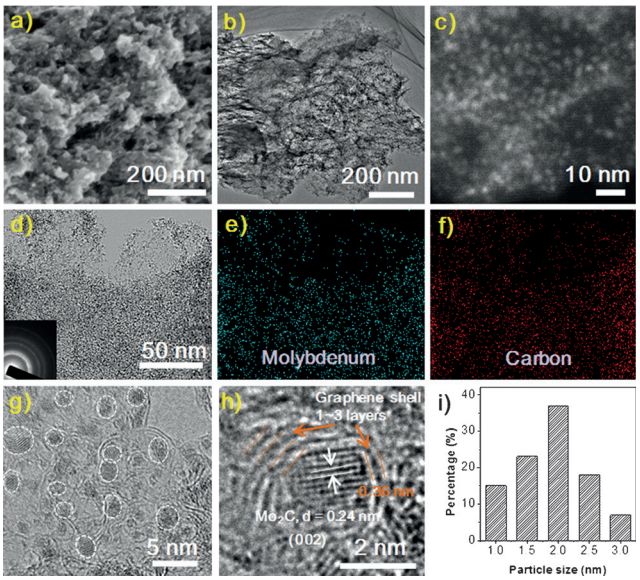

Figure 2. Analysis of Mo_2C NPs in MoDCA-5. a) SEM, b) TEM, c) HAADF STEM images. d–f) Simultaneously acquired TEM image (d; inset: SAED) and XEDS elemental mapping of molybdenum (e) and carbon (f). g,h) HRTEM images. i) Particle-size distribution.

extremely small nanometer diameters and that the carbon exists as ultrathin graphene layers with short-range order.[5d,12] Notably, no carbon was produced when pure *g*-C_3N_4 was used instead of MoO_x@*g*-C_3N_4 (see Figure S2),[13] thus confirming the key role of Mo in the catalytic growth of carbon from the decomposed intermediates at high temperature.[14]

For clarification, the as-prepared sample was named MoDCA-*x*, which indicates the mass ratio (*x*) of DCA and the Mo compound in the precursor. The resulting material MoDCA-5 had a loose, porous texture, as shown by SEM and TEM (Figure 2a,b). High-angle annular dark-field (HAADF) scanning transition electron microscopy (STEM) as well as TEM indicated the presence of numerous small nanocrystallites (Figure 2c,d). Selected-area electron diffraction (SAED) confirmed the polycrystalline nature of the material (inset of Figure 2d), and X-ray energy-dispersive spectroscopy (XEDS) elemental mapping indicated the uniform distribution of C and Mo elements, except for small amounts of N and O (Figure 2e,f; see also Figures S3 and S4 and Table S1 in the Supporting Information). The N doping is beneficial for improving the interaction of active sites with H^+.[6a] High-resolution TEM (HRTEM) images indicated that most Mo_2C NPs were encapsulated by graphene shells with short-range order (ca. 1–3 layers; Figure 2g,h). The NPs had a uniform size of generally less than 3 nm (Figure 2i) with a *d* spacing of 0.24 nm, which is ascribed to the (002) plane of Mo_2C. The high dispersion and ultrasmall size of the Mo_2C NPs are ascribed to the confining effect of the *g*-C_3N_4 matrix, which prohibits Mo_2C NPs from aggregation and/or excessive growth. The presence of free carbon in MoDCA-5 was also verified by Raman spectroscopy (see Figure S5), and the content of free carbon was 54.8%, as determined by thermogravimetic analysis (see Figure S6).

Figure 3a shows the polarization curves obtained for MoDCA-*x* and a blank glassy-carbon (GC) electrode, as well as the state-of-the-art catalyst 20% Pt/C (catalyst loading: 0.25 mg cm^{-2} on the surface of GC). The optimized annealing temperature was 800 °C owing to the smaller size of the Mo_2C NPs (see Figure S7). As expected, both bare GC and MoO_x@*g*-C_3N_4 showed very limited HER activity (Figure 3a; see also Figure S8). In sharp comparison, MoDCA-5 prepared at 800 °C had a very small U_{onset} value of approximately −6 mV (Figure 3a), which is very close to the thermodynamic potential of HER (i.e., 0 mV) as well as the U_{onset} value of

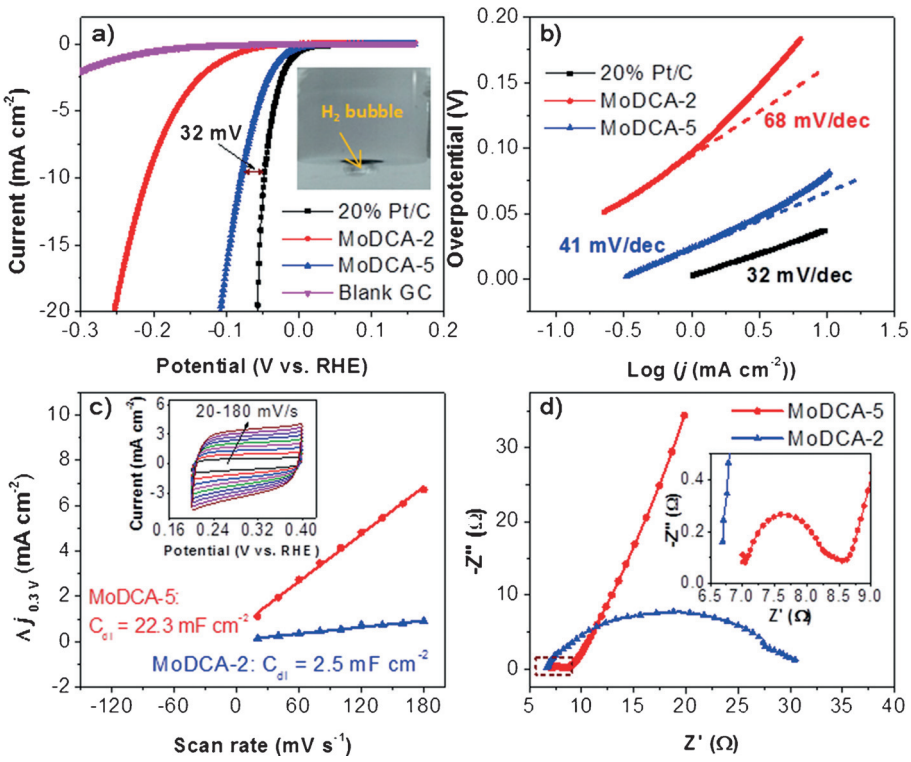

Figure 3. a) Polarization curves after *iR* compensation for a blank GC electrode, MoDCA-*x*, and 20% Pt/C in 0.5 M H_2SO_4 at a scan rate of 2 mV s^{-1} (inset: photograph showing the production of H_2 bubbles on the surface of MoDCA-5). b) Tafel plots of MoDCA-*x* and 20% Pt/C. c) Capacitive current at 0.3 V as a function of scan rate for MoDCA-*x* ($\Delta j_0 = j_a - j_c$; inset: cyclic voltammograms (CVs) for MoDCA-5 with different rates from 20 to 180 mV s^{-1} in the potential range of 0.2–0.4 V). d) Electrochemical impedance spectroscopy (EIS) Nyquist plots collected at a bias voltage of −150 mV for MoDCA-5 and −550 mV for MoDCA-2. RHE = reversible hydrogen electrode.

state-of-the-art 20% Pt/C, which is a benchmark HER electrocatalyst. A very small η_{10} value of 78 mV, only 32 mV larger than that for Pt/C, was required for MoDCA-5, thus indicating its exceptional HER electrocatalytic activity. In terms of η_{10}, MoDCA-5 is comparable to MoP | S (64 mV)[5b] and CoP NPs (75 mV),[6e] and significantly outperforms many other transition-metal-based HER electrocatalysts, including Mo_2C-based materials (140–192 mV), MoB (220 mV), MoP (90–150 mV), MoS_2 (180–200 mV), WS_2 (142–230 mV), WCN (220 mV), Co_2P (134 mV), Co@NCNTs (270 mV), Ni_2P (100 mV), and FeCo@NCNTs (280 mV), although it is somewhat inferior to metallic WO_2–C NWs (58 mV)[4a] and Ni_5P_4 NPs (23 mV)[8a] (see Table S2 for a detailed comparison). However, the mass loading for Ni_5P_4 as a compressed pellet is as high as 157 mg cm^{-2}.[8a] Moreover, a decrease in the DCA/ammonium molybdate mass ratio to 2 resulted in a larger U_{onset} value of −62 mV and η_{10} value of 205 mV for the resulting material MoDCA-2 than for MoDCA-5, thus indicating that MoDCA-5 is much superior in HER activity to MoDCA-2.

Further insight into the catalytic activity of MoDCA-*x* was obtained by extracting the slopes from the Tafel plots in Figure 3b ($\eta = b\log j + a$, in which b is Tafel slope, j is the current density, and a is the intercept relative to j_0).[15] The Tafel slope for commercial Pt/C is 32 mV dec^{-1}, which is smaller than the values of 41 and 68 mV dec^{-1} for MoDCA-5 and MoDCA-2, respectively. The smaller Tafel slope value of MoDCA-5 indicates its superior HER activity. These values also demonstrate that HER on MoDCA-*x* proceeds by a Volmer–Heyrovsky mechanism, in which the fast discharge of a proton is followed by rate-limiting electrochemical recombination with an additional proton.[8b] The j_0 value of MoDCA-5 was determined to be 0.178 mA cm^{-2}, and is thus over 10 times that of MoDCA-2 (0.017 mA cm^{-2}). The Tafel slope and j_0 values are both significantly superior to those of various Mo/W/Co/Ni-based HER electrocatalysts, such as MoB, Mo_2C, WS_2, Ni_2P, and Co_2P (see Table S2).

Both MoDCA-5 and MoDCA-2 are composed of ultrafine Mo_2C nanoparticles encapsulated by graphene layers (see Figure S9), but the HER activity of MoDCA-5 is higher than that of MoDCA-2. The difference in activity can be attributed to the following five points: a) Whereas MoDCA-2 exhibits a macroporous network of dense walls (see Figure S4), the loose texture of MoDCA-5 with hierarchical nanopores (13–20 nm, 102 nm) enables the ready, fast diffusion of the electrolyte into the small nanopores and thus the more efficient utilization of active sites in MoDCA-5 (see Table S3). b) The Brunauer–Emmett–Teller (BET) specific surface area (70 m^2 g^{-1}) of MoDCA-5 is 5 times that of MoDCA-2 (14 m^2 g^{-1}). Consequently, more catalytic sites should be accessible, thus resulting in the increased activity of MoDCA-5 (see Figure S10 and Table S3). c) The double-layer capacitance (C_{dl})—representing the electrochemically active surface area (ECSA)—of MoDCA-5 is 22.3 mF cm^{-2}: nearly 8 times as high as the value of 2.5 mF cm^{-2} for MoDCA-2 (Figure 3c; see also Figure S11). Thus, the large j_0 value of MoDCA-5 may be associated with its large ECSA as well as its large BET surface area.[16] d) The higher content of free carbon of MoDCA-5 (54.8%) as compared to MoDCA-2 (38.1%) could effectively lower the electrical resistance of MoDCA-5 (see Figure S6), thus promoting fast electron transport to active sites. Indeed, the electrical conductivity of MoDCA-5 (26.1 S cm^{-1}) is larger than that of MoDCA-2 (0.29 S cm^{-1}). e) MoDCA-5 has a significantly lower charge-transfer impedance (1.5 Ω) than MoDCA-2 (24 Ω), which leads to more facile electrode kinetics for MoDCA-5 toward HER (Figure 3d; see also Figure S12).

The HER performance of transition-metal-based materials is highly correlated with the chemical environment of the metal. The Mo 3d core level XPS spectra are split into $3d_{5/2}$ and $3d_{3/2}$ peaks because of spin–orbital coupling (Figure 4).

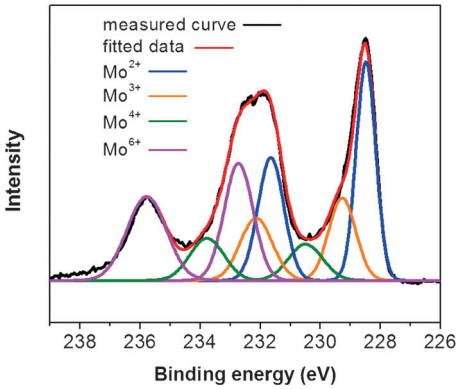

Figure 4. Mo 3d core level XPS spectrum of MoDCA-5.

The peak fitting of the Mo 3d XPS peak for MoDCA-5 suggests that there are four oxidation states (+2, +3, +4, and +6) for Mo on the surface of Mo_2C NPs. Mo^{4+} and Mo^{6+} are derived from MoO_2 and MoO_3, respectively, both of which are thought to be inactive for HER.[9a] It has been reported that the surface of Mo_2C NPs can be readily contaminated with molybdenum oxides when exposed to air.[17] Mo^{2+} and Mo^{3+} are assigned as carbides and nitrides, respectively,[17b,18] thus implying N doping of the Mo_2C nanoparticles. Moreover, the resulting graphene shells are also doped with some nitrogen atoms, which mainly exist in the form of pyridinic nitrogen atoms (see Figure S13). When MoO_x@*g*-C_3N_4 is annealed at 800 °C, the C,N-rich precursor not only acts as a carbon source to reduce MoO_x species to form carbides, but also provides nitrogen atoms, which are doped into Mo_2C and the graphene layers. After the electrochemical oxidation of Mo^{2+} and Mo^{3+} to Mo^{6+} on the surface of MoDCA-5 by scanning the potential up to 2.22 V, the HER activity was almost negligible (see Figure S14), which strongly implies that Mo^{2+} and Mo^{3+} species serve as the active sites in HER.[3a,5c,11,17b] Furthermore, this activity could be maintained with only a small loss of 20 mV at η_{10} after 2000 CV sweeps. About 93% of the catalytic current density was maintained after long-term durability testing for 12 h at a fixed overpotential of 78 mV. These results indicate the high stability of MoDCA-5 for HER (Figure 5).

The comprehensive HER performance of MoDCA-5 is among the highest observed for transition-metal-based electrocatalysts (see Table S2). Such superior HER activity has not even been observed for other Mo_2C-based electrocata-

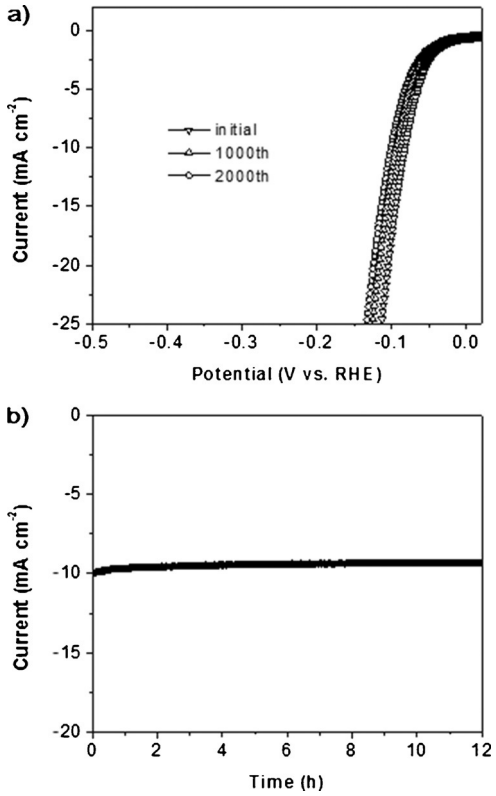

Figure 5. a) Polarization curves for MoDCA-5 initially and after 1000 and 2000 CV scans. b) Time-dependent current-density curve for MoDCA-5 at a static overpotential of 78 mV over 12 h.

lysts. The unique nanostructure of Mo_2C NPs encapsulated by ultrathin graphene shells can not only efficiently stop the aggregation and excessive growth of ultrafine Mo_2C NPs synthesized at high temperature, but can also reduce the electrical resistance between neighboring surface-oxide Mo_2C NPs. The former property is favorable for the exposure of more active sites for H^+ adsorption, whereas the latter helps improve electron transport to active sites. Moreover, the doping N atoms can not only interact with H^+ better than C atoms owing to the presence of long-pair electrons on the N atoms,[6a] but also favorably modify the electronic structures of adjacent Mo and C atoms, thus enhancing the interaction with H^+. Also, the ultrathin graphene shells can promote electron penetration from the Mo_2C core to the graphene surface[12,19] to improve reactivity for HER.

In summary, we have developed a one-step strategy for the controllable synthesis of uniform, ultrafine Mo_2C NPs, with sizes lower than 3 nm, encapsulated by ultrathin graphene shells (ca. 1–3 layers) by simply annealing a mixture of low-cost dicyanamide and ammonium molybdate. The resulting nanocomposite acted as a hydrogen-evolving electrocatalyst with superior activity and good long-term stability in an acidic medium. The superior HER activity can be attributed to the cooperative/synergistic effects of ultrafine Mo_2C NPs, ultrathin graphene shells, and N dopant. This effective method might be extended to the design and preparation of other carbide NPs (e.g. tungsten carbide@carbon; see Figure S15) for various electrocatalytic applications.

Acknowledgements

We are grateful for financial support from the Shanghai Institute of Ceramics, the Key Project for Young Researchers of the State Key Laboratory of High Performance Ceramics and Superfine Microstructure, the One Hundred Talent Plan of the Chinese Academy of Sciences, the National Natural Science Foundation of China (No. 21307145), the Youth Science and Technology Talents "Sail" Program of Shanghai Municipal Science and Technology Commission (No. 15YF1413800), and the Shanghai Government (Research Grant No. 14DZ2261200).

Keywords: electrocatalysis · graphene · hydrogen-evolution reaction · molybdenum carbide nanoparticles · water splitting

How to cite: *Angew. Chem. Int. Ed.* **2015**, *54*, 14723–14727
Angew. Chem. **2015**, *127*, 14936–14940

[1] a) H. M. Chen, C. K. Chen, R. S. Liu, L. Zhang, J. Zhang, D. P. Wilkinson, *Chem. Soc. Rev.* **2012**, *41*, 5654–5671; b) J. Kibsgaard, Z. Chen, B. N. Reinecke, T. F. Jaramillo, *Nat. Mater.* **2012**, *11*, 963–969.

[2] V. R. Stamenkovic, B. S. Mun, M. Arenz, K. J. J. Mayrhofer, C. A. Lucas, G. Wang, P. N. Ross, N. M. Markovic, *Nat. Mater.* **2007**, *6*, 241–247.

[3] a) M. S. Faber, S. Jin, *Energy Environ. Sci.* **2014**, *7*, 3519–3542; b) W.-F. Chen, S. Iyer, S. Iyer, K. Sasaki, C.-H. Wang, Y. Zhu, J. T. Muckerman, E. Fujita, *Energy Environ. Sci.* **2013**, *6*, 1818–1826; c) Z. Xing, Q. Liu, A. M. Asiri, X. Sun, *Adv. Mater.* **2014**, *26*, 5702–5707.

[4] a) R. Wu, J. Zhang, Y. Shi, D. Liu, B. Zhang, *J. Am. Chem. Soc.* **2015**, *137*, 6983–6986; b) H. Yan, C. Tian, L. Wang, A. Wu, M. Meng, L. Zhao, H. Fu, *Angew. Chem. Int. Ed.* **2015**, *54*, 6325–6329; *Angew. Chem.* **2015**, *127*, 6423–6427; c) M. A. Lukowski, A. S. Daniel, C. R. English, F. Meng, A. Forticaux, R. J. Hamers, S. Jin, *Energy Environ. Sci.* **2014**, *7*, 2608–2613; d) D. Voiry, H. Yamaguchi, J. Li, R. Silva, D. C. B. Alves, T. Fujita, M. Chen, T. Asefa, V. B. Shenoy, G. Eda, M. Chhowalla, *Nat. Mater.* **2013**, *12*, 850–855.

[5] a) M. A. Lukowski, A. S. Daniel, F. Meng, A. Forticaux, L. Li, S. Jin, *J. Am. Chem. Soc.* **2013**, *135*, 10274–10277; b) J. Kibsgaard, T. F. Jaramillo, *Angew. Chem. Int. Ed.* **2014**, *53*, 14433–14437; *Angew. Chem.* **2014**, *126*, 14661–14665; c) D. H. Youn, S. Han, J. Y. Kim, J. Y. Kim, H. Park, S. H. Choi, J. S. Lee, *ACS Nano* **2014**, *8*, 5164–5173; d) H. B. Wu, B. Y. Xia, L. Yu, X.-Y. Yu, X. W. Lou, *Nat. Commun.* **2015**, DOI: 10.1038/ncomms7512; e) J. M. McEnaney, J. C. Crompton, J. F. Callejas, E. J. Popczun, A. J. Biacchi, N. S. Lewis, R. E. Schaak, *Chem. Mater.* **2014**, *26*, 4826–4831.

[6] a) X. Zou, X. Huang, A. Goswami, R. Silva, B. R. Sathe, E. k. Mikmeková, T. Asefa, *Angew. Chem. Int. Ed.* **2014**, *53*, 4372–4376; *Angew. Chem.* **2014**, *126*, 4461–4465; b) S. Peng, L. Li, X. Han, W. Sun, M. Srinivasan, S. G. Mhaisalkar, F. Cheng, Q. Yan, J. Chen, S. Ramakrishna, *Angew. Chem. Int. Ed.* **2014**, *53*, 12594–12599; *Angew. Chem.* **2014**, *126*, 12802–12807; c) D. Kong, H. Wang, Z. Lu, Y. Cui, *J. Am. Chem. Soc.* **2014**, *136*, 4897–4900; d) Z. Huang, M. G. Humphrey, C. Zhang, Z. Chen, Z. Chen, C. Lv, *Nano Energy* **2014**, *9*, 373–382; e) E. J. Popczun, C. G. Read, C. W. Roske, N. S. Lewis, R. E. Schaak, *Angew. Chem. Int. Ed.* **2014**, *53*, 5427–5430; *Angew. Chem.* **2014**, *126*, 5531–5534.

[7] P. Jiang, Q. Liu, Y. Liang, J. Tian, A. M. Asiri, X. Sun, *Angew. Chem. Int. Ed.* **2014**, *53*, 12855–12859; *Angew. Chem.* **2014**, *126*, 13069–13073.

[8] a) A. B. Laursen, K. R. Patraju, M. J. Whitaker, M. Retuerto, T. Sarkar, N. Yao, K. V. Ramanujachary, M. Greenblatt, G. C. Dismukes, *Energy Environ. Sci.* **2015**, *8*, 1027 – 1034; b) E. J. Popczun, J. R. McKone, C. G. Read, A. J. Biacchi, A. M. Wiltrout, N. S. Lewis, R. E. Schaak, *J. Am. Chem. Soc.* **2013**, *135*, 9267 – 9270.

[9] a) H. Vrubel, X. Hu, *Angew. Chem. Int. Ed.* **2012**, *51*, 12703 – 12706; *Angew. Chem.* **2012**, *124*, 12875 – 12878; b) W. F. Chen, C. H. Wang, K. Sasaki, N. Marinkovic, W. Xu, J. T. Muckerman, Y. Zhu, R. R. Adzic, *Energy Environ. Sci.* **2013**, *6*, 943 – 951; c) L. Liao, S. Wang, J. Xiao, X. Bian, Y. Zhang, M. D. Scanlon, X. Hu, Y. Tang, B. Liu, H. H. Girault, *Energy Environ. Sci.* **2014**, *7*, 387 – 392.

[10] Y. Zhao, K. Kamiya, K. Hashimoto, S. Nakanishi, *J. Am. Chem. Soc.* **2015**, *137*, 110 – 113.

[11] W.-F. Chen, J. T. Muckerman, E. Fujita, *Chem. Commun.* **2013**, *49*, 8896 – 8909.

[12] J. Deng, P. Ren, D. Deng, X. Bao, *Angew. Chem. Int. Ed.* **2015**, *54*, 2100 – 2104; *Angew. Chem.* **2015**, *127*, 2128 – 2132.

[13] X. C. Wang, K. Maeda, A. Thomas, K. Takanabe, G. Xin, J. M. Carlsson, K. Domen, M. Antonietti, *Nat. Mater.* **2009**, *8*, 76 – 80.

[14] Y. Jia, L. He, L. Kong, J. Liu, Z. Guo, F. Meng, T. Luo, M. Li, J. Liu, *Carbon* **2009**, *47*, 1652 – 1658.

[15] A. B. Laursen, S. Kegnæs, S. Dahl, I. Chorkendorff, *Energy Environ. Sci.* **2012**, *5*, 5577 – 5591.

[16] D. Merki, S. Fierro, H. Vrubel, X. Hu, *Chem. Sci.* **2011**, *2*, 1262 – 1267.

[17] a) M. Xiang, D. Li, W. Li, B. Zhong, Y. Sun, *Catal. Commun.* **2007**, *8*, 513 – 518; b) C. Wan, Y. N. Regmi, B. M. Leonard, *Angew. Chem. Int. Ed.* **2014**, *53*, 6407 – 6410; *Angew. Chem.* **2014**, *126*, 6525 – 6528.

[18] a) S. Dong, X. Chen, K. Zhang, L. Gu, L. Zhang, X. Zhou, L. Li, Z. Liu, P. Han, H. Xu, *Chem. Commun.* **2011**, *47*, 11291 – 11293; b) J. M. Horn, Z. Song, D. V. Potapenko, J. Hrbek, M. G. White, *J. Phys. Chem. B* **2005**, *109*, 44 – 47.

[19] G. Wu, K. L. More, C. M. Johnston, P. Zelenay, *Science* **2011**, *332*, 443 – 447.

Received: July 23, 2015
Published online: October 16, 2015

